Correlating the microstructure of thin films of poly[5,5-bis(3-dodecyl-2-thienyl)-2,2-bithiophene] with charge transport: Effect of dielectric surface energy and thermal annealing

Leslie H. Jimison,[1] Alberto Salleo,[1,*] Michael L. Chabinyc,[3] David P. Bernstein,[2,4] and Michael F. Toney[4]
[1]*Department of Materials Science, Stanford University, Stanford, California 94305, USA*
[2]*Department of Applied Physics, Stanford University, Stanford, California 94305, USA*
[3]*Palo Alto Research Center, 3333 Coyote Hill Road, Palo Alto, California 94304, USA*
[4]*Stanford Synchrotron Radiation Laboratory, Menlo Park, California 94025, USA*
(Received 15 April 2008; published 16 September 2008)

Poly[5,5′-bis(3-dodecyl-2-thienyl)-2,2′-bithiophene] (PQT-12) is a conjugated polymer that shows promising performance ($\mu > 0.1$ cm^2/V s) as a semiconductor for thin-film electronics. The electrical properties of PQT-12 thin films can vary by over 3 orders of magnitude depending on the chemistry of the substrate onto which they are deposited and on annealing conditions. The highest mobility is obtained in films annealed on a dielectric treated with a self-assembled monolayer of octadecyltrichlorosilane (OTS). Polymeric thin films were processed from either a solution of dissolved PQT-12 molecules in 1,2-dichlorobenzene or from a nanoparticle dispersion of the polymer in the same solvent (nPQT-12). In addition, the substrate surface chemistry was altered by spin coating on a bare SiO_2 dielectric or on SiO_2 treated with OTS. The microstructure of the two forms of polymer, as characterized using specular and grazing x-ray diffraction in addition to rocking curves, was compared and correlated with the electrical performance of the films as active layers in thin-film transistors. As-spun films of nPQT-12 are always more crystalline than those of PQT-12, independent of substrate chemistry. Consequently, carrier mobility in as-spun films is higher in nPQT-12 than in PQT-12. The presence of the OTS monolayer at the polymer/dielectric interface increases crystallinity of both PQT-12 and nPQT-12, without significantly affecting their texture. After annealing, the mobility in PQT-12 films and nPQT-12 films is comparable. Annealing causes the polymer films on OTS to undergo crystallite growth in the direction normal to the substrate. In nPQT-12, growth of the crystalline coherence length in the π-π stacking direction (i.e., parallel to the substrate and in the direction of charge transport) occurs as well. The mobility increase in nPQT-12 on OTS upon annealing is thus attributed to the higher crystallinity of the film. In PQT-12 films deposited on OTS on the other hand, annealing causes a decrease in the out-of-plane misorientation of neighboring crystallites without any significant grain growth in the plane of the film. The mobility increase in PQT-12 on OTS upon annealing is attributed to a better intergrain connectivity, in agreement with electrical modeling of the transistor characteristics using a mobility edge model.

DOI: 10.1103/PhysRevB.78.125319 PACS number(s): 73.50.−h, 72.80.Le, 73.61.Ph

I. INTRODUCTION

Rigid rod semiconducting polymers have drawn much interest because of their use in light emitting diodes,[1] photovoltaic cells,[2] and thin-film transistors (TFTs).[3,4] All of these applications rely on the charge carrying ability of thin films of these polymers. Molecular organization and longer range ordering have a strong impact on the electrical properties of semiconducting polymers. For example, transport in layered alkylated conjugated polymers is highly anisotropic.[5,6] Adjacent semiconducting backbones are poorly coupled electronically through the insulating side chains and well coupled cofacially due to overlap of their π orbitals. The orientation of the molecules relative to the direction of transport thus has a strong influence on their ability to transport charge. Our ability to arbitrarily control the crystalline texture of these films to maximize the mobility of carriers for a given device has proven to be extremely limited.[7] Understanding how these materials order on different types of substrates, e.g., those with different surface functionalities or different roughness, is essential to improve our control of the electrical properties.

Electrical transport in TFTs is strongly dependent on the microstructure of the semiconducting layer.[4,5] The microstructure, in part, determines the electronic density of states (DOS) through which carriers move. The most widely studied semicrystalline polymer used in TFTs is poly(3-hexylthiophene) (P3HT).[6,8,9] Previous studies have shown that the field-effect mobility of carriers in P3HT depends on the nature of the semiconductor-dielectric interface,[10–12] the molecular weight of the polymer,[13–17] and the conditions used for film formation such as solvent[18] and drying time.[19] The molecular weight influences the crystallinity and also the connectivity between these domains.[13–16] Most TFTs are fabricated using spin coating; this coating method is known to form films with microstructures that can be kinetically limited due to the short drying time. Finally, it is found that, in general, hydrophobic gate dielectric layers produce higher performance TFTs than those fabricated with hydrophilic dielectrics.[4,20]

P3HT has been used extensively as a model system to understand ordering in thin films of conjugated polymers. Semicrystalline polymer thin films have a heterogeneous microstructure comprising small (approximately 10 nm) crystallites and amorphous regions. In the crystalline areas, P3HT orders such that the conjugated backbones are coupled by π stacking in one dimension and are separated in the other by the alkyl side chains.[21,22] The side chains have been

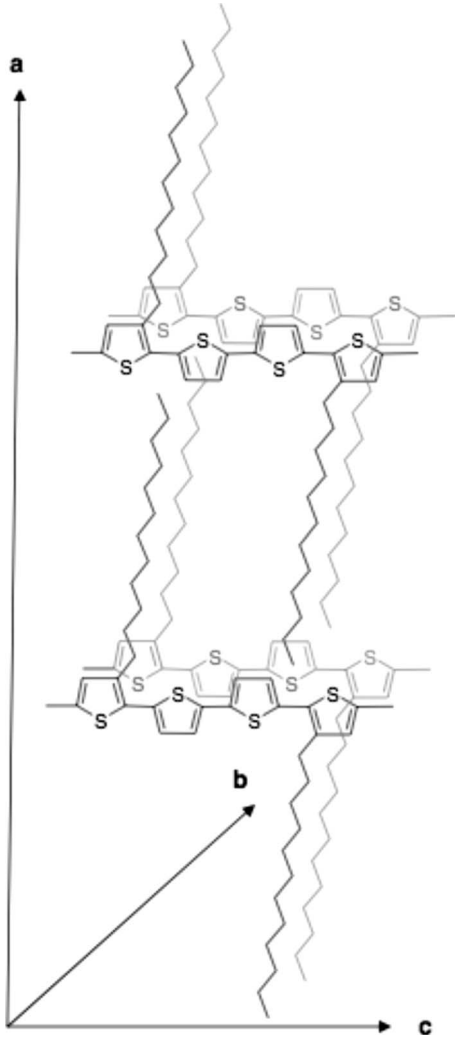

FIG. 1. Structure of PQT-12 crystallites.

shown to be relatively disordered, that is, they comprise linear alkyl chains with gauche conformational defects.[23] Little evidence for order in the third dimension, along the backbone, is observed in x-ray scattering from thin films. Typically these ordered regions are textured relative to the surface normal; they are either found with the π-stacking direction predominantly in the plane of the substrate or perpendicular to it.[6,10] Within the plane of the substrate, the films are isotropic. The out-of-plane texturing has been shown to depend on the molecular weight, the substrate, and the casting solvent.[11–13,15,16] These differences in microstructure have been connected with the electrical properties; for example, if the backbone and the π-stacking directions are in the plane where current flows, the mobility is generally higher as opposed to a structure where the alkyl chain direction lies in such a plane. Atomic force microscopy (AFM) has shown that the surface of these films can display domains of π-stacked molecules when the polydispersity is well controlled.[17]

Poly[5,5′-bis(3-dodecyl-2-thienyl)-2,2′-bithiophene] (PQT-12) has the same conjugated backbone as P3HT (see Fig. 1) but generally has a higher field-effect mobility.[24–27] In PQT-12 the density of the 12 atom alkyl side chain along the backbone is half that of P3HT. Unlike P3HT, during thermal annealing PQT-12 undergoes a thermal transition that allows for reordering in thin films and in powder form. More specifically, PQT-12 shows two thermal transitions in differential scanning calorimetry data that have been attributed to phase transitions of the crystal-to-liquid crystal (~120 °C) and the liquid crystal to melt (150 °C). The material can be processed either as a homogeneous solution at low concentrations (PQT-12)[24] or from a "nanoparticle" dispersion (nPQT-12) at higher concentrations.[25] The dispersed solution comprises a mixture of dissolved PQT-12 and aggregates of PQT-12. The average particle size reported for nPQT-12 solutions is 10 nm.[25] The two forms differ only in the processing conditions used to form the casting solution and both can be made with polymers of the same molecular weight (typically ~30 kDa). Films formed from nPQT-12 have a higher mobility as cast compared to those of PQT-12; however both formulations have similar performance after annealing above 120 °C.[28,29] Mobility data of nPQT-12 and PQT-12 as a function of processing conditions are summarized in Table I.

TABLE I. Mobility of PQT-12 and nPQT-12 films processed in different conditions.

	Mobility ($cm^2/V\ s$)	
	PQT-12	nPQT
As cast on SiO_2/OTS	0.004	0.01
Annealed on SiO_2/OTS	0.1	0.06
As cast on SiO_2	No measurable field effect	0.01
Annealed on SiO_2	0.0002–0.0005	0.001–0.006

There are no reports of the detailed crystallographic structure of PQT-12. Based on molecular models and low-resolution diffraction data, the basic packing structure has been assumed to be as shown in Fig. 1. According to this model, lamellar stacking due to the alkyl side chains occurs along the *a* axis, the π-stacking direction is along the *b* axis, and repeat units of the polymer lie along the *c* axis. The peak positions of the methylene stretches measured by infrared spectroscopy show that the side chains are relatively well ordered after annealing and are only slightly more disordered prior to annealing supporting the fully extended side chains shown in the figure.[30] Based on density considerations, the side chains are interdigitated and the backbones are π stacked.[31] This simple packing model is consistent with most of the reported experimental data and likely captures the relevant features of the packing that can be used to understand the crystalline order in the films.

Transport in PQT-12 TFTs has been extensively examined and used to infer details about the nature of the electronic structure of films. Charge transport, as characterized by field-effect mobility in TFTs, depends dramatically on the chemistry of the dielectric/semiconductor interface and on thermal treatments of the films (Table I).[26,28,29] It is found that depending on the specific processing conditions, mobility can vary over many orders of magnitude. The temperature dependences of mobility in PQT-12 and P3HT were previously modeled with a mobility edge (ME) model.[29,32] In the ME

TABLE II. ME fitting parameters of PQT-12 as a function of thermal treatments and dielectric surface chemistry.

	μ_0 ($cm^2/V\,s$)	E_b (eV)	N_{tot} (cm^{-3})
PQT-12 on OTS/SiO_2 as cast	1–4	50	5.5×10^{20}
PQT-12 on OTS/SiO_2 annealed	1–4	34	6.5×10^{20}
PQT-12 on bare SiO_2 annealed	0.05	50	1.7×10^{21}

model, a demarcation energy E_{ME} is defined that separates mobile states from traps (the ME). Mobile states have a constant mobility μ_0 and trap states are assumed to have zero mobility. Due to structural disorder, states are found in the forbidden gap. For simplicity the DOS in the gap is often modeled as an exponential tail characterized by a total number of trap states N_{tot} and a characteristic width E_b. As a result, the DOS of the trap states is

$$D_{traps}(E) = \frac{N_{tot}}{E_b}\exp\left(-\frac{E}{E_b}\right), \tag{1}$$

where the energy is measured from the top of the valence band and is taken as positive in the band gap.

In the ME model, the measured effective mobility is the average mobility of all carriers, trapped and free. With increasing $|V_G|$ the fraction of holes in mobile states increases and so does the effective mobility.[33] When temperature is decreased on the other hand, the effective mobility at constant V_G decreases. It is indeed commonly observed in all semicrystalline polymers that the mobility increases with increasing charge density and decreases with decreasing temperature.

The ME model links carrier transport to the microstructure of the film. Structural defects may appear as states in the gap, which act as traps. The ME model has been successfully applied to *a*-Si:H and poly-Si thin films.[34,35] In poly-Si thin films, for instance, broader trap distributions have been associated with smaller-grained material. Similarly, in *a*-Si:H, the effect of deposition temperature on mobility has been explained by different trap distributions. Details of the electrical measurements of PQT-12 and their modeling using the ME model are found in Ref. 29. By applying the ME model to PQT-12, it was found that thermal annealing did not significantly affect the crystalline mobility μ_0 or the total trap density while it had a profound effect on the trap energy distribution (Table II). Upon annealing, the gap state distribution was found to have a tighter energy distribution, as demonstrated by the decrease in E_b. The dielectric surface chemistry on the other hand had an effect on both μ_0 and E_b. Fabricating devices on bare SiO_2 rather than octadecyltrichlorosilane (OTS)-treated SiO_2 caused a decrease in μ_0 and a broadening of the trap state distribution (i.e., an increase in E_b).

Nevertheless, the effect of processing on microstructure is still poorly understood. For instance, phase contrast in tapping mode atomic force microscopy has been reported to show that spin-coated PQT-12 films on bare SiO_2 have a different morphology than those on OTS-coated SiO_2.[26,27] These differences are relatively small when compared to the large difference in field-effect mobility on the two substrates. Here we attempt to connect the previously described results from the ME model with changes in the microstructure of the PQT-12 thin film studied by x-ray diffraction. Moreover, we will compare the microstructure of PQT-12 thin films with that of nPQT-12.

This paper is organized as follows. We will first explain the experimental details of our measurements. We will then describe the results from synchrotron-based x-ray diffraction of PQT-12 as a function of thermal treatment and of dielectric surface treatment. Results from similar experiments carried out on nPQT-12 will be presented next. Finally, we will discuss how the observed changes in the microstructure of these materials correlate with their electrical characterization.

II. EXPERIMENT

A. Materials

Poly[5,5′-bis(3-dodecyl-2-thienyl)-2,2′-bithiophene] was obtained from Xerox Research Centre of Canada in two forms, a solid (PQT-12) and a dispersion (nPQT-12) in 1,2-dichlorobenzene.[24,25] The solid was dissolved in 1,2-dicholorbenzene (~5 mg/ml) and filtered while hot through a 1 μm polytetrafluoroethylene syringe filter prior to spin coating. The dispersion was used as received.

B. Fabrication of the films

Thin films of PQT-12 and nPQT-12 were spin coated at 500–1000 rpm onto silicon wafers with a thin native oxide layer. The substrates were cleaned by exposure to a low power oxygen plasma prior to spin coating the film. Self-assembled monolayers (SAMs) of OTS were formed on the oxide using a previously reported procedure (OTS/SiO_2).[20] The resulting films were typically ~30–100 nm in thickness. Films were thermally annealed on a hot plate under nitrogen and cooled to room temperature by switching off the hot plate and allowing it to cool.

C. X-ray scattering measurements

Measurements of x-ray scattering were performed at the Stanford Synchrotron Radiation Laboratory on beamlines 2–1 (high-resolution specular scattering), 7–2 (high-resolution grazing incidence scattering with a point detector), and 11–3 [two-dimensional (2D) scattering with an area detector, MAR345 image plate, at grazing and specular incidences]. Data are expressed as a function of the scattering vector, $\mathbf{q}$. We resolve this into components in the substrate plane and normal to the substrate plane, $\mathbf{q}_{xy}$ and $\mathbf{q}_z$, respectively. $\mathbf{q}$ has a magnitude of $(4\pi/\lambda)\sin\theta$, where θ is half the scattering angle and λ is the wavelength of the incident radiation; the lattice spacing corresponding to a diffraction peak, d, is simply equal to $2\pi/\mathbf{q}$.[36] The incident energies were 8 keV for beamlines 2–1 and 7–2 and 12.7 keV for 11–3. In some runs, the samples were kept under a helium atmosphere during irradiation to minimize damage to the films from the intense x-ray beam; beam damage of the

samples generally resulted in a decrease in scattering intensity but no change in the position of peaks. Typical exposure times for measurements made using the area detector were 20–30 min. The data for out-of-plane scattering were corrected for the area of illumination by multiplication by theta, the incident angle. For the grazing incidence x-ray scattering (GIXS), the films were illuminated at incidence angles of about 0.2° for 8 keV (7–2 measurements) and about 0.12° for 12.7 keV (11–3 measurements). These values were chosen so that the x-ray beam penetrates the entire thickness of the polymer sample (~30–100 nm) but only a portion (<20 nm) of the silicon substrate.[36,37] This choice reduces the background scattering from the substrate. The high-resolution GIXS data were corrected for the area of illumination based on the slits used for the incident and exiting beam and sample size.[38] Due to constraints of time on the beamlines, all types of scans were not performed on all samples.

Since we used several beamlines and detectors for these experiments, it is important to understand the resolution of each one to best compare complementary data. The resolution of the data obtained with the point detector is determined by the collimation on the detector. For the high-resolution specular scattering (beamline 2–1), the collimation was set by a Ta-doped Si(111) crystal with an angular width of about 0.01° (or a resolution of about 0.001 $Å^{-1}$ for the scattering vector, $\mathbf{q}$), while for the high-resolution grazing incidence scattering (beamline 7–2), it was set by 1 mrad Soller slits (effectively 0.1° or a $\mathbf{q}$ resolution of 0.007 $Å^{-1}$). The resolution of the data obtained using the image plate detector is coarser than that obtained with the point detector and is determined by the sample size (1.5×1.5 cm), the distance between the sample and the detector (ranging from 39 to 41 cm), and the detector pixel size (150×150 μm). The resolution varies as a function of $\mathbf{q}$ but is less than 0.1 $Å^{-1}$ over the range of interest.

For texture measurements of the (100) and (200) peaks (rocking scans) using the image plate detector, we used the following procedure to measure these low Bragg angle (~1.5° and 3°) peaks. An approximate incidence (Bragg) angle was calculated from the position of the diffraction peaks in the specular data. Since this position is only approximate (due to lack of resolution) and we were not confident of the absolute value of the incident angle, we would rock the sample by 0.2° about the nominal (calculated) Bragg angle while imaging of the scattering. This procedure ensured that we captured the Bragg diffraction peak within the rocking motion.

III. RESULTS

A. PQT-12 on OTS/SiO_2

1. 2D survey patterns

Shown in Fig. 2 are the 2D grazing angle diffraction patterns from PQT-12, both (a) as spun and (b) after annealing. In the diffraction pattern of the as-spun film, two orders of peaks corresponding to the $\mathbf{a}^*$ reciprocal-lattice direction pointing approximately along the $\mathbf{q}_z$ axis. We have indexed these as the (100) and (200) peaks caused by diffraction along the alkyl stacking direction. It should be noted that because of the geometry of the experiment, the peaks seen along the nominal $\mathbf{q}_z$ axis are due to off-specular diffraction and do not reflect the true intensity profile in reciprocal space of the corresponding Bragg peaks (at $\mathbf{q}_{xy}=0$). Weaker peaks along the $\mathbf{q}_{xy}$ axis are also visible. The most intense of these features is a peak near $\mathbf{q}_{xy}=1.7$ $Å^{-1}$; this scattering wave vector corresponds to the π-π stacking distance between two cofacial polymer chains (~3.7 Å). A broad ring due to diffraction from disordered material is visible at $\mathbf{q}_{xy}\approx 1.5$ $Å^{-1}$ as well. Figure 2(b) shows the 2D grazing angle diffraction pattern from the same film after annealing for 20 min at 140 °C. The (100) peak intensifies, shifts to higher $\mathbf{q}_z$, and sharpens, losing some of the broadening that is present in the as-spun material. The (200) peak becomes considerably more intense, and a (300) peak is clearly visible. As before, all (h00) peaks lie along the nominal $\mathbf{q}_z$ axis. More peaks along $\mathbf{q}_{x,y}$ axis are present as well. The peak located at $\mathbf{q}_{x,y}=1.7$ $Å^{-1}$ increases in intensity upon annealing, while the disorder peak at $\mathbf{q}=1.5$ $Å^{-1}$ disappears. Several mixed-index peaks off the $\mathbf{q}_z$ and $\mathbf{q}_{x,y}$ axes appear as well. It should be noted that the mixed-index peaks and the (h00) peaks are not aligned horizontally showing that the lattice is not orthorhombic.

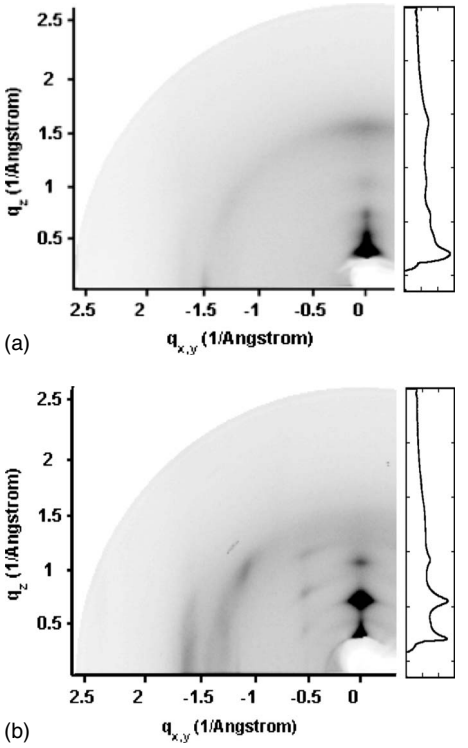

FIG. 2. 2D survey diffraction patterns of PQT-12 films on OTS/SiO_2 (a) as spun and (b) annealed. The plots on the right of the diffraction patterns are vertical line scans (intensity vs $\mathbf{q}_z$) extracted at $\mathbf{q}_{xy}\sim 0$.

2. High-resolution grazing incidence and specular diffraction patterns

To complement 2D survey data, grazing incidence and specular diffraction patterns were collected using a point de-

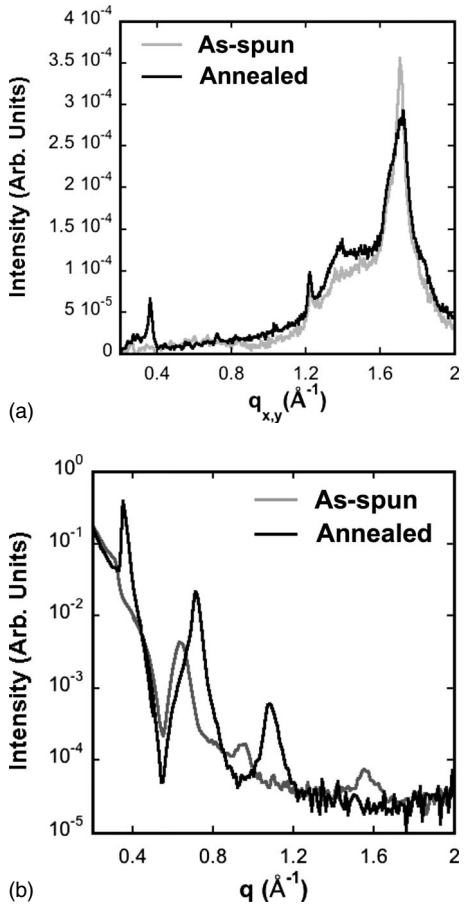

FIG. 3. High-resolution (a) grazing incidence and (b) specular diffraction patterns of annealed and as-spun PQT-12 films on OTS/SiO_2 substrate.

tector, with higher angular resolution and greater sensitivity (Fig. 3). In Fig. 3(a), the grazing incidence patterns for the as-spun and annealed films are shown. In both patterns an intense peak appears at the π-stacking distance of approximately 3.7 Å. The high angular resolution in these measurements shows that the peak at $\mathbf{q}_{xy}=1.7$ Å^{-1} in the 2D images can be deconvoluted into two components centered at $\mathbf{q}_{xy}=1.68$ and 1.72 Å^{-1}. Two more peaks are observed at $\mathbf{q}_{xy}$ of 1.22 and 1.4 Å^{-1}. A broad feature spanning from $\mathbf{q}_{xy}=1.2$ Å^{-1} to $\mathbf{q}_{xy}=2$ Å^{-1} is also present; because this feature is substantially wider than the other peaks, it is likely due to scattering from disordered regions in the film. Except for the broad 1.2–2 Å^{-1} feature, which was fitted with a Gaussian, the diffraction peaks could be well fitted with Lorentzians. Peak positions and full width at half maximum (FWHM) are given in Table III. Interestingly, the as-spun and the annealed films have very similar grazing incidence diffraction patterns. The only notable change brought about by thermal annealing is the appearance of a weak alkyl stacking peak at $\mathbf{q}_{xy}=0.36$ Å^{-1}. The d spacing of the π-π stacking in PQT-12 shows a sample-to-sample variation of about 0.2 Å prior to annealing but it is the same for all samples after annealing. Grazing incidence patterns obtained from $\mathbf{q}_z=0$ slices of the 2D data confirm that the intensity of the π-π stacking peak remains essentially unchanged on annealing.

The positions and FWHMs of the diffraction peaks in the specular direction [Fig. 3(b)] are summarized in Table IV. In the specular diffraction of the as-spun film, a peak at $\mathbf{q}_z=0.305$ Å^{-1} corresponding to the first-order alkyl stacking, (100), barely emerges above the background. Because the background (due to the reflectivity from the polymer-substrate interface) drops sharply with diffraction angle, the (200) and (300) peaks, however, are well defined. These latter two peaks give an average d spacing of 19.8 Å. A weak peak at $\mathbf{q}_z=1.55$ Å^{-1} is likely due to diffraction from amorphous material and thus corresponds to the broad ring observed in Fig. 2(a). Upon annealing, all peaks move to higher $\mathbf{q}$, increase in intensity, and decrease in width giving an average d spacing of 17.5 Å in agreement with previously determined value (18 Å) from lower-resolution experiments.[24,25] The disorder peak at $\mathbf{q}_z\approx 1.5$ Å^{-1} is no longer present in agreement with the 2D diffraction data. Finally, the (200) peak is a convolution of two peaks, one located at the $\mathbf{q}$ value where the corresponding peak was found in the as-spun material and the other at a slightly larger value of $\mathbf{q}$. Although this observation indicates that the (100) peak should be composed of two peaks, we cannot resolve them due to the close proximity of the peaks and the high background scattering at low q. A corresponding very weak shoulder also appears to be present near the (300) peak.

3. Rocking curves

To further investigate crystallite orientation, the profiles of the peaks in $\mathbf{q}$ space were measured by wide-angle and high-resolution rocking curves (Fig. 4). The use of the area detector in Bragg geometry allows one to determine the shape of the diffraction peaks in reciprocal space. Quantitative information is obtained by extracting line scans from the diffraction peak and subtracting the background from off the diffraction condition, giving the wide-angle rocking curves. The (100) peak of the as-spun film has a FWHM of ~3.55° but has wings that span a 20° range [Fig. 4(a)]. Upon annealing, the FWHM of the peak decreases to 3.15° and the wings of the peak are suppressed by almost 1 order of magnitude. A high-resolution rocking curve of the annealed film reveals the existence of an extremely narrow peak having an instrument-limited FWHM of approximately 0.01° and a maximum intensity higher than that of the scattering away from surface normal by a factor of approximately 50. No high-resolution rocking curve of the (100) peak was measured for the as-spun film, as it was too difficult to determine the exact location of this peak in specular diffraction geometry. The wide-angle rocking curve of the (200) peak of the as-spun PQT-12 film barely emerges from the background [Fig. 4(b)]. A higher-intensity resolution-limited peak however is detected with the high-resolution rocking curve measurement, in agreement with the observation of a well-resolved specular diffraction peak [Fig. 3(b)]. Annealing significantly increases both the intensities of the broad diffraction peak and that of the narrow central peak, respectively, by factors of 20 and 15.

B. nPQT-12 on OTS/SiO_2

1. 2D survey patterns

As shown in Fig. 5, the 2D image of the scattering at grazing incidence on nPQT-12 is similar to that of PQT-12

TABLE III. Positions, intensities, and FWHM of the diffraction peaks in the GIXS spectra of nPQT-12 and PQT-12. The absolute intensities for nPQT-12 and PQT-12 films are different due to alignment and film thickness differences between runs.

Material and condition	Index	**Q** (1/Å)		Amplitude		FWHM (1/Å)	
		nPQT-12	PQT-12	nPQT-12	PQT-12	nPQT-12	PQT-12
As-spun OTS		1.219	1.224	0.0002	0.000 66	0.10	0.024
		1.37	1.368	0.0002	0.000 23	0.10	0.122
		1.512		0.001		0.046	
	010	1.6508	1.649	0.001	0.000 63	0.06	0.028
	010	1.705	1.708	0.0017	0.003 16	0.066	0.05
		1.82	1.789	0.002	9×10^{-5}	0.05	0.01
140 °C OTS		1.219	1.221	0.0018	0.000 14	0.014	0.018
		1.353	1.394	0.0015	0.0002	0.060	0.08
		1.512		0.0006		0.06	
	010	1.6508	1.684	0.004	0.001 24	0.048	0.095
	010	1.71	1.724	0.0038	0.001 35	0.060	0.04
		1.82	1.83	0.001	0.000 32	0.080	0.1
As-spun SiO_2		1.22		0.0003		0.08	
		1.36		0.0002		0.1	
		1.51		0.002		0.05	
	010	1.65		0.001		0.064	
	010	1.71		0.002		0.058	
		1.80		0.0005		0.12	
140 °C SiO_2		1.219	1.221	0.0015	0.000 135	0.014	0.018
		1.353	1.394	0.0015	0.000 212	0.060	0.09
		1.512		0.0007		0.07	
	010	1.6508	1.675	0.0048	0.000 84	0.048	0.08
	010	1.71	1.72	0.005	0.000 59	0.054	0.04
		1.82	1.83	0.001	0.000 22	0.080	0.1

TABLE IV. Positions, intensities, and FWHM of the diffraction peaks in the specular patterns of nPQT-12 and PQT-12. The absolute intensities for nPQT-12 and PQT-12 films are different due to alignment and film thickness differences between runs.

Substrate and annealing	Index	**Q** (1/Å)		Amplitude		FWHM (1/Å)	
		nPQT-12	PQT-12	nPQT-12	PQT-12	nPQT-12	PQT-12
As spun on OTS	(100)		0.305		0.037		0.0435
	(200)	0.673	0.637	0.015	0.004	0.104	0.069
	(300)	1.01	0.949	0.000 47	0.0001	0.106	0.057
140 °C on OTS	(100)	0.3604	0.359	1.8	1.96	0.012	0.013
	(200)	0.727	0.719	0.043	0.07	0.016	0.023
	(300)	1.095	1.08	0.0007	0.0016	0.035	0.037
As spun on oxide	(100)	0.346	0.344	0.109	0.017	0.054	0.045
	(200)	0.687		0.0014		0.084	
140 °C on oxide	(100)	0.361	0.354	3.8	0.043	0.011	0.0127
	(200)	0.723	0.726	0.18	0.000 75	0.022	0.0321
	(300)	1.086	1.09	0.005	9.8×10^{-5}	0.046	0.04

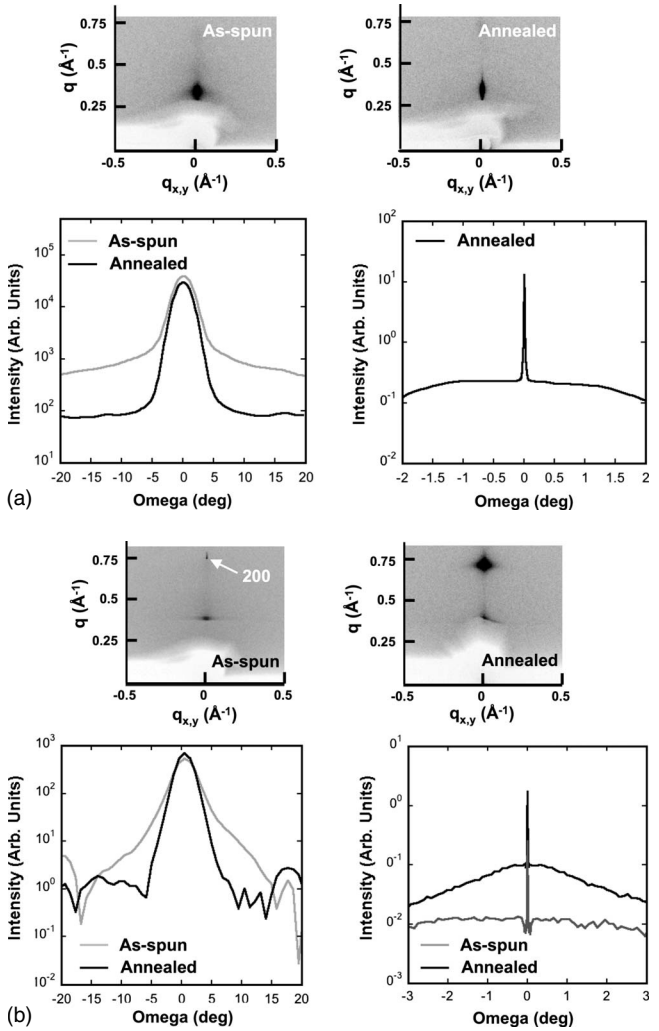

FIG. 4. (a) (100) Bragg peak of PQT-12 film as spun and annealed on OTS/SiO_2 (top panel), accompanied with corresponding line scans. High-resolution rocking curve data are shown in the bottom left panel (annealed film only). (b) (200) Bragg peak of PQT-12 film as spun and annealed on OTS/SiO_2 (top panel), accompanied with corresponding line scans. High-resolution rocking curve data are shown in the bottom right panel.

with the largest differences between the two materials arising in the as-cast films. As-cast films of nPQT-12 have strong texturing, with the a^* axis oriented along the $\mathbf{q}_z$ direction. There are multiple peaks nominally along the $\mathbf{q}_{xy}$ direction suggesting that the as-spun films of nPQT-12 have in-plane crystalline order. Upon annealing, the peaks along the $\mathbf{q}_z$ axis become sharper and off-axis peaks appear in the pattern. These peaks are indicative of three-dimensional order in the annealed film due to improved registry of the polymer chains.

2. High-resolution grazing incidence and specular diffraction patterns

The ordering process was examined in more detail using high-resolution data along $\mathbf{q}_{xy}$. There are similar peaks on as-cast films and annealed ones, but the relative intensities of these peaks change after annealing (Fig. 6 and Tables III and IV). In both the as-spun and annealed films, there are two closely spaced peaks (1.65 and 1.71 Å^{-1}) that have d spacings corresponding to π-stacking distances (3.81 and 3.66 Å). The intensity of the peak at 1.65 Å^{-1} is higher than that at 1.71 Å^{-1} unlike in films of PQT-12. There are also peaks at $\mathbf{q}_{x,y}$ equal to 1.22, 1.36, 1.51, and 1.8 Å^{-1}; to fit the scattering profile with these peaks, the inclusion of a broad peak centered at ~1.45 Å^{-1} is also required similar to films of PQT-12. The largest change in the as-cast and annealed films is the intensity of the peaks at $\mathbf{q}_{xy}$=1.65 and 1.71 Å^{-1} significantly increases, while that of the peak at $\mathbf{q}_{xy}$ =1.51 Å^{-1} decreases slightly. The change in intensity suggests that this peak may be due to ordered domains in the as-spun film that are recrystallizing into a different structure in agreement with the changes observed in the lamellar spacing. The widths of the peaks are similar in annealed films except for that of the peak at $\mathbf{q}_{xy}$=1.21 Å^1 that is approximately four times narrower.

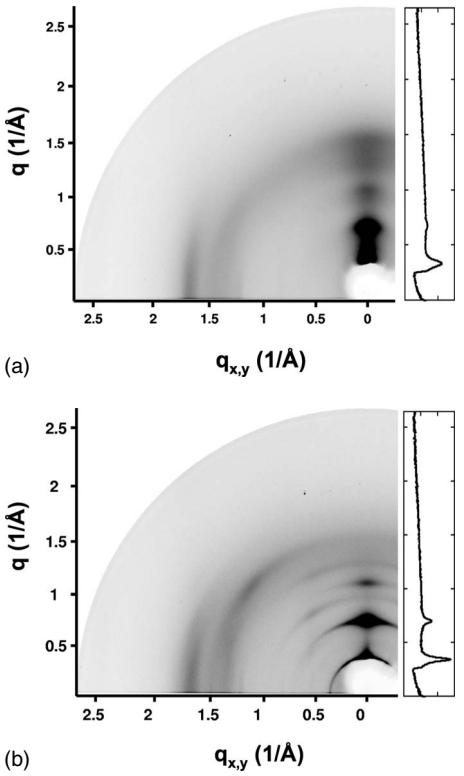

FIG. 5. 2D survey diffraction patterns of nPQT-12 films on OTS/SiO_2 (a) as spun and (b) annealed. The plots on the right of the diffraction patterns are vertical line scans (intensity vs $\mathbf{q}_z$) extracted at $\mathbf{q}_{xy} \sim 0$.

High-resolution specular scans, along $\mathbf{q}_z$, were performed to determine the lamellar spacing more precisely. After spin casting, films of nPQT-12 typically show two orders of a Bragg peak corresponding to lamellar stacking. In many cases, the background reflectivity near the (100) peak has significant intensity so it is difficult to determine the parameters of the peak accurately. In most films, the (200) peak can be clearly resolved from the background so we use it to determine a d spacing of 18.7 Å for the a axis. After annealing at 130–140 °C followed by a slow cooling, films of nPQT-12 show stronger specular scattering, a shift of the

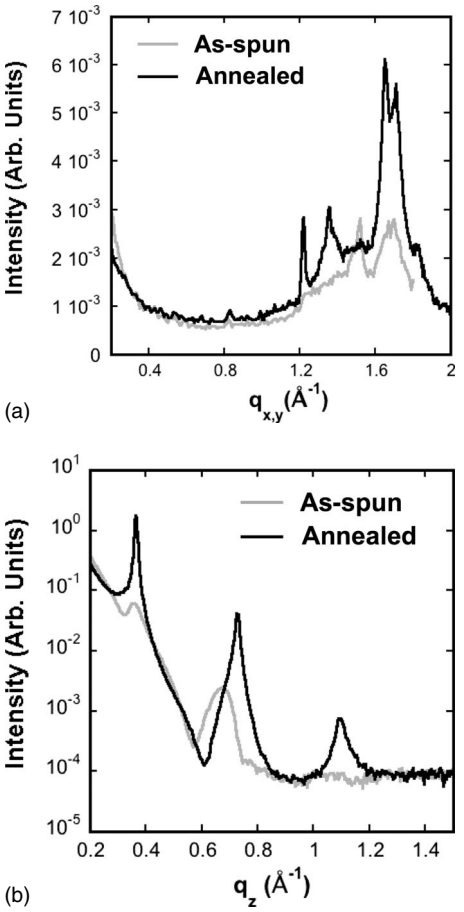

FIG. 6. High-resolution (a) grazing incidence and (b) specular diffraction patterns of annealed and as-spun nPQT-12 films on OTS/SiO_2 substrate.

peaks to a smaller d spacing, and narrowing of the peak width. The d spacing of the lamellar stacking is 17.3 Å based on an average of the d spacing of the three peaks.

3. Rocking curves

The rocking curves of the (200) peak of films of nPQT were measured for the as-spun and annealed films (Fig. 7). The (200) peaks were examined using the area detector as described previously. The angular profile of the (200) peak in the as-spun film has a strong narrow peak near the surface normal (ω=0°) with a broader scattering feature (FWHM of 13°) at its base. Upon annealing at 140 °C, the broad peak grows more intense with an increase in the scattering away from the surface normal (FWHM of 9°). The central feature is still observed in the annealed film and does not change shape. High-resolution measurements of the (200) peak of an annealed film show that there is an intense peak at the surface normal with a width that is $<$0.01°, the limit of resolution for those data. The intensity of this peak is approximately ten times higher than the broad component away from ω=0°.

C. PQT-12 on bare SiO_2

1. 2D survey patterns

The 2D diffraction patterns of PQT-12 films as spun and annealed on bare oxide are shown in Fig. 8. Trends similar to

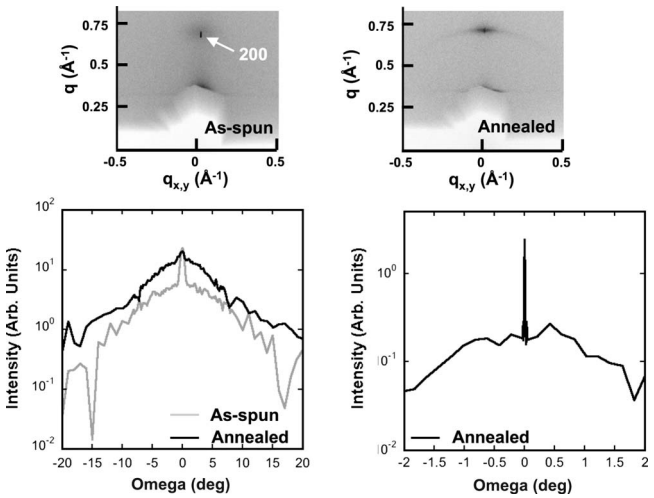

FIG. 7. (200) Bragg peak of nPQT-12 film as spun and annealed on OTS/SiO_2 (top panel), accompanied with corresponding line scans (bottom panel). High-resolution rocking curve data are shown in the bottom right panel (only annealed film).

those seen for the films on OTS are observed. The as-spun scan reveals two (h00) peaks along the $\mathbf{q}_z$ axis and a very faint peak along the $\mathbf{q}_{xy}$ axis. Upon annealing, the (h00) peaks sharpen and intensify, revealing the presence of a third order (h00) peak. The peaks along $\mathbf{q}_{xy}$ intensify and mixed-index peaks appear.

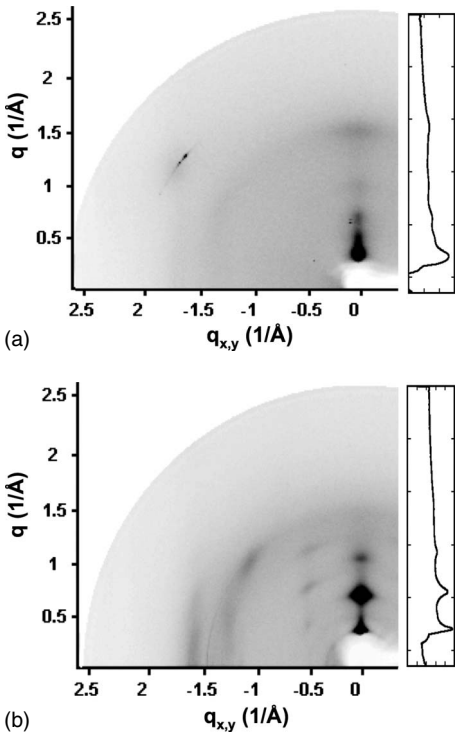

FIG. 8. 2D survey diffraction patterns of PQT-12 films on bare SiO_2 (a) as spun and (b) annealed. The plots on the right of the diffraction patterns are vertical line scans (intensity vs $\mathbf{q}_z$) extracted at $\mathbf{q}_{xy} \sim 0$.

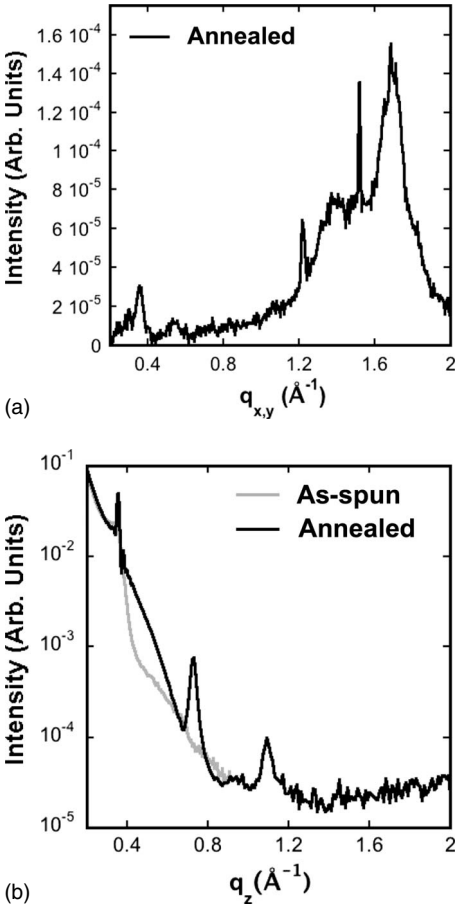

FIG. 9. High-resolution (a) grazing incidence of annealed PQT-12 film and (b) specular diffraction patterns of annealed and as-spun PQT-12 films on bare SiO_2 substrate.

2. High-resolution grazing incidence and specular diffraction patterns

The high-resolution grazing incidence pattern of annealed PQT-12 on SiO_2 is essentially similar to that on OTS/SiO_2 (Table III). The π-stacking peak at $\mathbf{q}_{xy}=1.7$ Å^{-1} dominates [Fig. 9(a)] and can be deconvoluted in two peaks centered at $\mathbf{q}_{xy}=1.68$ and 1.72 Å^{-1}. A broad peak attributed to scattering form disordered materials is visible between $\mathbf{q}_{xy}=1.2$ Å^{-1} and $\mathbf{q}_{xy}=2$ Å^{-1}. A poorly defined (100) peak is also visible at $\mathbf{q}_{xy}=0.36$ Å^{-1}. The very sharp feature at $\mathbf{q}=1.5$ Å^{-1} remains unidentified

The specular diffraction scan of the unannealed PQT-12 film shows only a weak (100) peak [Fig. 9(b)]. Upon annealing, (100), (200), and (300) peaks develop. Their positions and FWHM are reported in Table III. The surface of the film used for the measurements was particularly uniform, allowing for the appearance of finite-thickness fringes, most clearly visible on either side of the (100) peak. By measuring the fringe spacing, Δ, the thickness of the annealed PQT-12 film on oxide can be estimated according to the following equation:

$$\frac{2\pi}{\Delta} = t. \tag{2}$$

The film thickness obtained from the thickness fringes is approximately 34 nm, in good agreement with film thickness measured by AFM (40 nm).

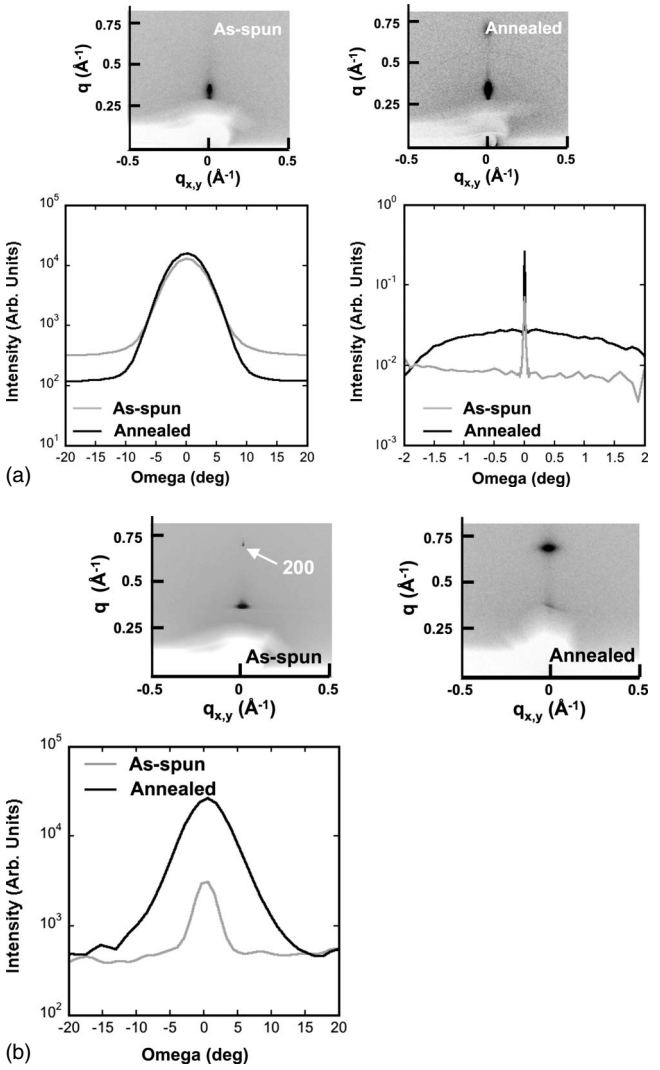

FIG. 10. (a) (100) Bragg peak of PQT-12 film as spun and annealed on bare SiO_2 (top panel), accompanied with corresponding line scans. High-resolution rocking curve data are shown in the bottom right panel. (b) (200) Bragg peak of PQT-12 film as spun and annealed on bare SiO_2 (top panel), accompanied with corresponding line scans. High-resolution rocking curve data did not show the presence of a resolution-limited peak and is therefore not displayed.

3. Rocking curves

On annealing, the rocking curve of the (100) Bragg peak [Fig. 10(a)] shows a slight increase accompanied by a decrease in the off-normal scattering intensity. The effect is more pronounced in the (200) wide-angle rocking curve, where on annealing there is a large increase in peak intensity and FWHM. Both the as-spun and annealed films display a resolution-limited narrow central peak in the (100) high-resolution rocking curves. Annealing increases the intensity of this peak by approximately a factor of 24. In the (200) high-resolution rocking curve, however, the resolution-limited peak was not observed.

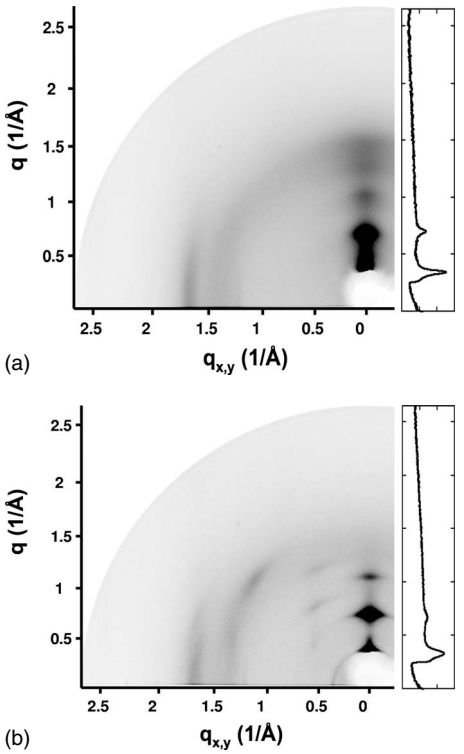

FIG. 11. 2D survey diffraction patterns of nPQT-12 films on bare SiO_2 (a) as spun and b) annealed. The plots on the right of the diffraction patterns are vertical line scans (intensity vsq_z) extracted at $q_{xy} \sim 0$.

D. nPQT-12 on bare SiO_2

1. 2D survey patterns

The 2D image of the scattering at grazing incidence on nPQT-12 on bare SiO_2 is substantially similar to that on OTS/SiO_2 (Figs. 5 and 11). After annealing, the scattering pattern of the film becomes more complex with the appearance of more peaks and a sharpening of the peaks along the $\mathbf{q}_z$ axis. These features are at the same positions as those of the film on OTS/SiO_2.

2. High-resolution grazing incidence and specular diffraction patterns

High-resolution grazing incidence scattering along the $\mathbf{q}_{xy}$ direction shows that there are similar peaks in as-cast and annealed films of nPQT-12 on bare oxide [Fig. 12(a)]. There are two closely spaced peaks (1.65 and 1.71 $Å^{-1}$) as observed for the films on OTS/SiO_2 with the former having a higher intensity in the annealed films. There are also peaks at $\mathbf{q}_{xy}$ equal to 1.22, 1.36, 1.51, and 1.8 $Å^{-1}$; to fit the scattering profile with these peaks, the inclusion of a broad peak at $\sim$1.45 $Å^{-1}$ is also required. After annealing, the widths of the peaks are slightly narrowed, but the changes are relatively small ($\sim$20%). The widths of the peaks are also nearly the same as those for films on OTS/SiO_2.

High-resolution specular scans were performed to determine the lamellar spacing more precisely [Fig. 12(b)]. In the as-cast films on SiO_2 the polymer-substrate reflectivity near the (100) peak has significant intensity, similar to films on OTS/SiO_2, and so it is difficult to resolve this peak accurately. The background near the (200) peak is smaller so it can be clearly resolved to yield a *d* spacing of 18.7 Å for the *a* axis. After annealing the film at 140 °C followed by a slow cooling, three orders of diffraction from the lamellar stacking can be resolved. The *d* spacing of the lamellar stacking in the annealed films is 17.3 Å, showing a densification of the packing along (100) after annealing.

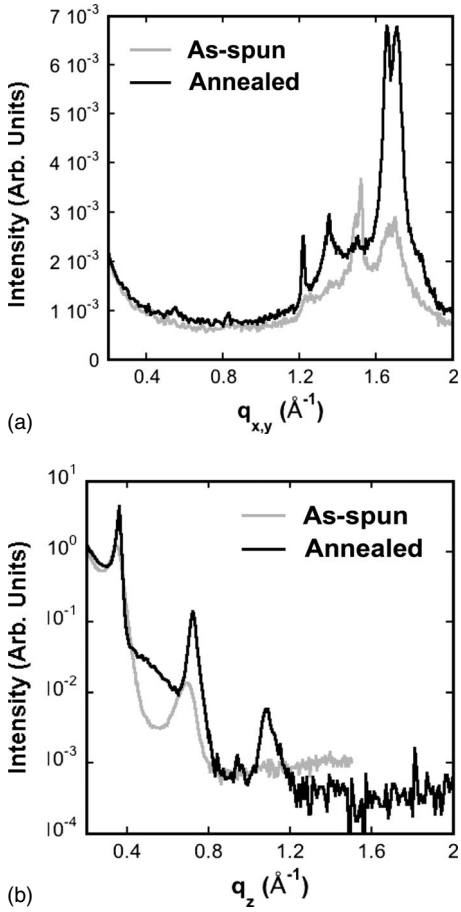

FIG. 12. High-resolution (a) grazing incidence and (b) specular diffraction patterns of annealed and as-spun nPQT-12 films on bare SiO_2 substrate.

3. Rocking curves

The rocking curves of the (100) and (200) peaks of films of nPQT on SiO_2 were examined in as-spun and annealed films (Fig. 13). Images of the scattering of the (200) peak in an as-spun film show again a strong narrow peak near the surface normal (ω=0°) with a broader background (FWHM of 12°) at its base along an arc with respect to the surface normal. Upon annealing at 140 °C, the scattering away from the surface normal (FWHM of 7°) increases in intensity. The central feature is still present, but the scattering away from ω=0° is nearly as intense partially obscuring the feature. High-resolution data for the (200) peak of an annealed film show that there is an intense resolution-limited peak at ω=0°. The intensity of this peak is approximately ten times higher than intensity from the misoriented crystallites away

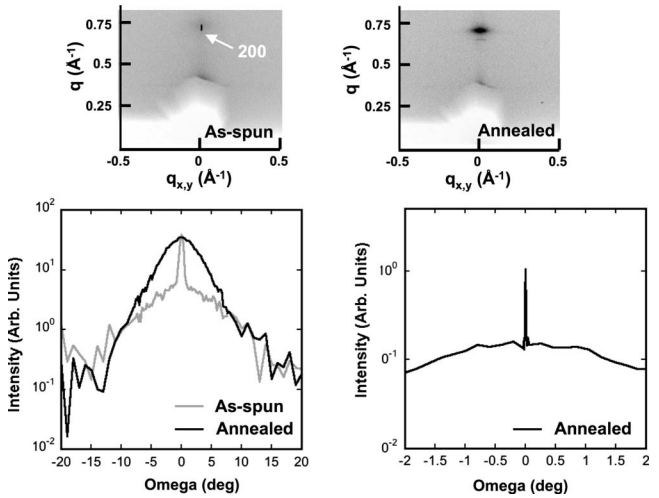

FIG. 13. (200) Bragg peak of nPQT-12 film as spun and annealed on bare SiO_2 (top panel), accompanied with corresponding line scans. High-resolution rocking curve data are shown in the bottom right panel (only annealed film).

from $\omega=0°$. Similar data for the (100) peak show that this resolution-limited peak is present in both the as-spun and annealed films.

E. Complete pole figures of PQT-12 and nPQT-12

Because the films are isotropic in the plane of the substrate, pole figures are completely represented by two axes rather than by a stereographic projection. By appropriately combining information from high-resolution rocking curves, wide-angle rocking curves, and 2D GIXS scattering, complete pole figures can be constructed. The intensity for the innermost angles, approximately 4° on either side of the peak, is obtained from the high-resolution rocking data. The intensity extending from 4° to approximately 20° is a line scan extracted at the **q** value of the (200) pole from the wide-angle rocking curve. For omega angles greater than approximately 20°, the intensity is represented by a line extraction at the **q** value of the (200) pole of the 2D GIXS data. The high-resolution rocking data are normalized with respect to film thickness. Data obtained from the wide-angle rocking curve are multiplied by a constant factor to match the normalized high-resolution rocking data and a similar procedure is used at the connection between the wide-angle rocking data and the 2D GIXS data. Smooth transitions are ensured by verifying that there are significant data overlaps at the intersection between the different data sets. A more detailed description of the geometric factors of the scattering experiments, which are not relevant for our purposes since they are the same for all samples, as well as a study of the quantitative use of pole figures to estimate percentage of film crystallinity, is outside the scope of this paper and will be discussed in a separate publication.

Shown in Figs. 14 and 15 are, respectively, the (200) pole figures of PQT-12 and nPQT-12 films as spun on OTS/SiO_2 and annealed on SiO_2 and OTS/SiO_2. These pole figures can be compared because they are normalized with respect to

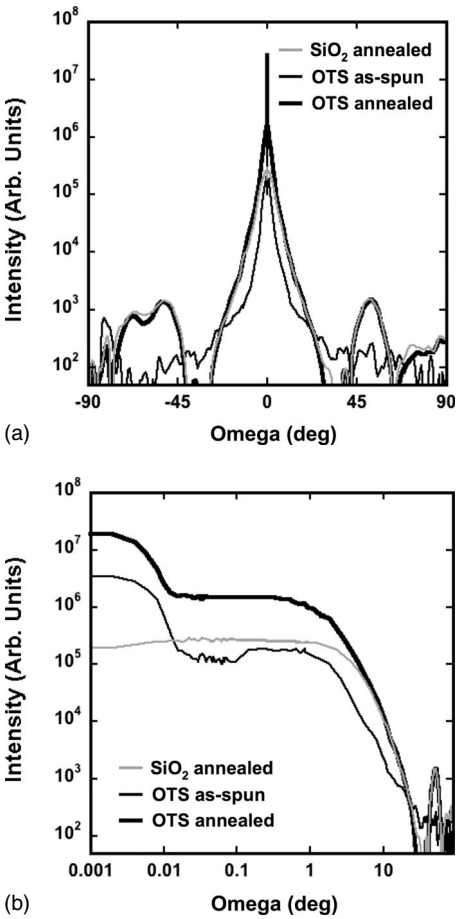

FIG. 14. (a) (200) pole figure of PQT-12 obtained for different processing conditions. In (b) the pole figure is plotted using a logarithmic scale for the rocking angle in order to emphasize the crystallite populations.

thickness. In these figures, we distinguish three populations of crystallites. "Perfectly oriented" crystallites are such that they contribute to the intensity of the pole figure at $\omega=0°$. The true orientational spread of this population of crystallites cannot be determined as the FWHM of this component of the pole figure is limited by the angular resolution of the instrument, but it is quite small ($<0.01°$). There is a second population of crystallites, which we define as "well oriented." The orientational spread of these crystallites is approximately $\pm 5°$ about the substrate normal. Finally, there are domains oriented at larger angles relative to the surface normal ($\omega > \sim 20°$) that we refer to as isotropic. Pole figures for both nPQT-12 and PQT-12 on OTS/SiO_2 show intensity contributions from perfectly oriented and well-oriented crystallites, regardless of heat treatment. Films of nPQT-12 and as-spun films of PQT-12 show measurable diffracted intensity at higher angles due to isotropic crystallites. Annealed films of PQT-12 on OTS/SiO_2 or bare SiO_2 on the other hand do not show any measurable scattering at $\omega > \sim 20°$. No resolution-limited peak from perfectly oriented crystallites is observed for PQT films on SiO_2.

It should be added that the intensity increase observed in the pole figures at $\omega \sim 55°$ is not due to misoriented (200) crystallites but rather to a mixed-index peak that is clearly

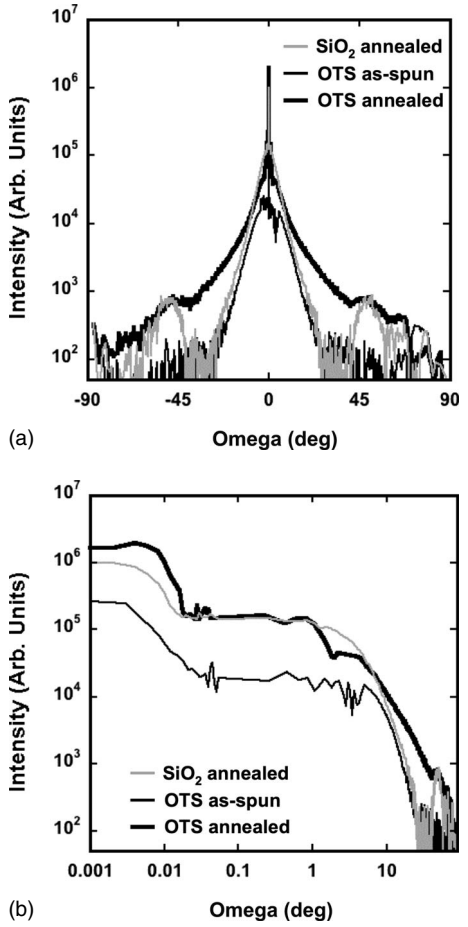

FIG. 15. (a) (200) pole figure of nPQT-12 obtained for different processing conditions. In (b) the pole figure is plotted using a logarithmic scale for the rocking angle in order to emphasize the crystallite populations. The noise floor is slightly higher than in Fig. 14 due to a different data averaging procedure.

visible at the same **q** as the (200) peak in Figs. 2(b), 8(b), and 11(b). These are the first pole figures reported for polymer thin films and they greatly aid in interpretation of the microstructural effects we observe.

IV. DISCUSSION

A. Effect of annealing

As-spun films of both PQT-12 and nPQT-12 on bare SiO_2 and on OTS/SiO_2 exhibit the typical thin-film texture of polythiophenes where the alkyl side chains stack in the direction normal to the substrate, indicated by the $(h00)$ peaks lying along the $\mathbf{q}_z$ axis.[6] The preferred crystallite texture is further emphasized by the (200) pole figure for the as-spun films. The pole figure has a sharp central peak arising from perfectly oriented crystallites and wings from the well-oriented population. The scattering from isotropic crystallites is relatively weak for both nPQT-12 and PQT-12 illustrating the preferred, although not perfect, out-of-plane texture of the crystallites in the as-spun films.

On annealing, regardless of the surface treatment, the crystalline quality of the films of PQT-12 and nPQT-12 improves, leading to more intense and well-defined peaks along the $\mathbf{q}_{xy}$ and $\mathbf{q}_z$ axes. The appearance of new off-axis peaks shows the formation of three-dimensional crystallites where there is registry of the backbones, rather than the layered structure typical of liquid-crystalline materials. This organization has been suggested previously based mainly on the molecular structure.[24] This three-dimensional structure is supported by the infrared-absorption frequencies of the methylene alkyl side chains that suggest that they are in a nearly all transconformation.[30] The positions of the mixed-index peaks in the 2D image of the x-ray scattering indicate that the unit cell is not orthorhombic because they do not lie on simple layer lines relative to the $(h00)$ peaks. We were unable to index all of the observed peaks simultaneously with a primitive monoclinic unit cell that is consistent with the molecular dimensions of the repeat unit of PQT-12. We therefore believe that the unit cell is likely triclinic if there is a unique crystalline form. It is also possible that there are two polymorphs leading to the observed pattern. The d spacing of the alkyl stacking changes after annealing without a substantial change in the peak positions along $\mathbf{q}_{xy}$ suggesting that there may be multiple polymorphs with only small variations in overall structure. Determination of the true molecular packing in the unit cell requires a combination of molecular simulation and structure factor calculations that is beyond the scope of this work.

Some information about the change in molecular packing after annealing can be inferred from the data without a detailed packing structure. Significant changes are observed in the specular diffraction patterns of both PQT-12 and nPQT-12 upon annealing: the $(h00)$ peaks intensify, shift to larger $\mathbf{q}_z$, and narrow. The shift to larger $\mathbf{q}_z$ of all the Bragg peaks after annealing corresponds to a decrease in interplanar spacing. Such densification has been observed in other rigid-rod polymers after thermal annealing.[39] The molecular packing in the as-spun films represents a kinetically limited structure that is dictated by the time required for evaporation of the solvent. It is likely that the flexible alkyl side chains are disordered in the as-cast films. By heating the films into a liquid-crystalline mesophase, the side chains become mobile allowing them to shift into a more closely stacked arrangement upon cooling. Due to their sparse spacing along the backbone, the side chains are able to interdigitate into an ordered crystal upon annealing to maximize the film density.[24,30,39] Interestingly, in some annealed films the $(h00)$ peaks can be fit with a superposition of two sets of $(h00)$ peaks at different values of **q** [Figs. 3(b), 6(b), and 12(b)]. The presence of two d spacings in the annealed films suggests that the two distances correspond to two polymorphic crystalline structures of PQT-12 and nPQT-12. One of the two structures corresponds to that of as-spun PQT-12 and the other is assumed to be the lower-energy configuration obtained after annealing. The difference in d spacing between the initial domains and the annealed ones is relatively small (~ 1 Å) and could easily be caused by small changes in the ordering of the alkyl side chains (e.g., the tilt of the side chains relative to the backbone or the extent of interdigitation).

The width of the lamellar $(h00)$ peaks can be used to estimate the size of the crystalline domains in the lamellar

direction. According to established broadening models, a constant value of Δq with respect to h would indicate that peak broadening is dominated by strain or crystallite size in the diffraction direction considered. The FWHMs of the (h00) peaks of the as-spun films of PQT-12 and nPQT-12 on OTS show no systematic dependence on order. In this case, the Scherrer formula can be applied to give a crystallite size of approximately 16 nm in the film thickness direction. In contrast, the width of the peaks in the annealed films shows a systematic increase with order. A linear relationship between Δq and h indicates that part of the broadening is due to variation in interplanar spacing between adjacent grains (nonuniform strain).[40] A linear relationship between Δq and h^2 indicates that part of the broadening originates from paracrystalline disorder: a variation in the interplanar spacing within the grains that do not average to zero.[40] Due to the limited number of (h00) peaks in the specular patterns, Δq may appear to vary linearly with both h or h^2. The intercept B at $h=0$, however, is related to the crystallite coherence length L_c along the diffraction direction (normal to the substrate surface) by Eq. (3),

$$L_c = 0.86x\frac{2\pi}{B}. \tag{3}$$

The value of L_c extracted from the linear fits of Δq as a function of h or h^2 must therefore be physically meaningful (e.g., positive and not greater than the film thickness) and can be used to discern the applicability of the peak broadening models. For the two annealed PQT-12 samples, there appears to be a linear relationship between Δq and h; however, this fit yields unphysical negative intercepts. Linear fits of Δq vs h^2 yield intercepts that are positive and correlate well with physical parameters of our films. The linear fit is better for the PQT-12 film annealed on OTS/SiO_2 than for that of the PQT-12 film annealed on bare SiO_2 [Fig. 16(a)]. The estimated crystallite size for the annealed film on bare SiO_2 using this intercept is approximately 47 nm, which is in fair agreement with the thickness extracted previously from finite-thickness fringes and AFM measurements. For the annealed PQT-12 film on OTS, the $h^2=0$ intercept provides an estimate of the crystallite dimension in the direction normal to the substrate of 70 nm. AFM measurements on the same film confirmed a thickness of approximately 100 nm. The extrapolated dimensions of the crystallites in both annealed films strongly suggest that the crystallites present span the entire thickness of the film or nearly so from the substrate interface to the air interface. Similar results are obtained for nPQT films on both OTS/SiO_2 and SiO_2 and thicknesses of 87 and 106 nm are obtained [Fig. 16(b)]. The variation in the thickness of the films is due to both the spin-coating conditions and the different concentrations used in the PQT-12 and nPQT-12 solutions.

Thus it has been established that crystallites grow to span the entire thickness of the PQT-12 and nPQT-12 films on annealing. However, such crystallite growth in the direction normal to the substrate surface does not explain how annealing improves the charge transport in TFTs. Crystallite growth perpendicular to the substrate is a characteristic of the entire film, but charge transport in thin-film devices occurs in-plane

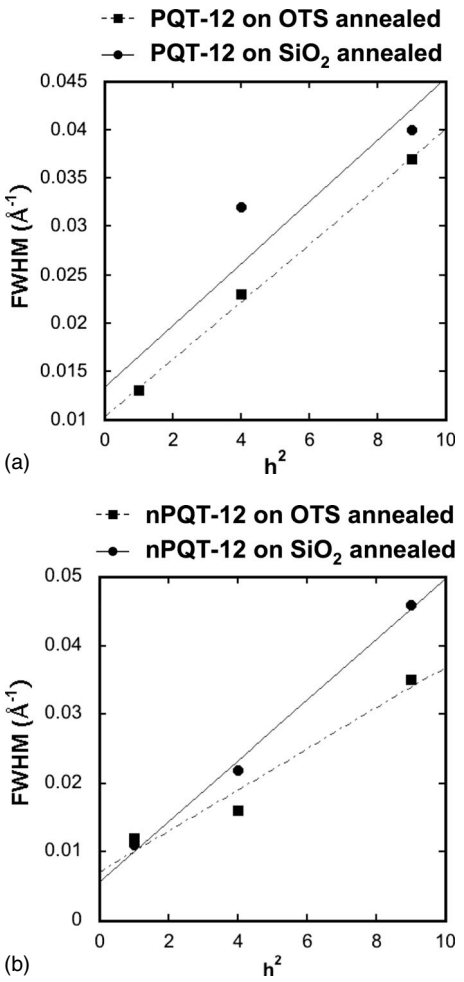

FIG. 16. FWHM of (h00) peaks as a function of h^2 for (a) PQT-12 and (b) nPQT-12.

within approximately 1 nm of the dielectric interface.[41] Improvements in charge transport are expected to be reflected by noticeable changes in the microstructure in the plane of the film. However, interestingly, the grazing incidence scans for the as-spun and annealed films of PQT-12 are nearly identical while those of nPQT-12 show an increase in diffracted intensity upon annealing. For PQT-12, there are no large changes in either intensity or peak width of the π-stacking peak. This implies that on annealing there is little change in the crystallite coherence length along the substrate.

The rocking curves of the lamellar peaks accompanied by the (200) pole figures of PQT-12 on OTS/SiO_2 help us to clarify the physical mechanisms that cause the mobility increase upon annealing. All of these curves show resolution-limited peaks, a feature attributed to the lateral coherence of the layered domains of perfectly oriented crystallites.[42] It has been previously inferred that this population of perfectly oriented crystallites is nucleated at the dielectric surface.[10,38] Without influence of an interface, crystallites nucleated in the bulk would likely have a much wider angular range; crystallites nucleated at the polymer/air interface would also exhibit an angular range considerably larger than the instrument resolution limit because of the surface roughness of the polymer film. Only the dielectric/polymer interface is smooth enough

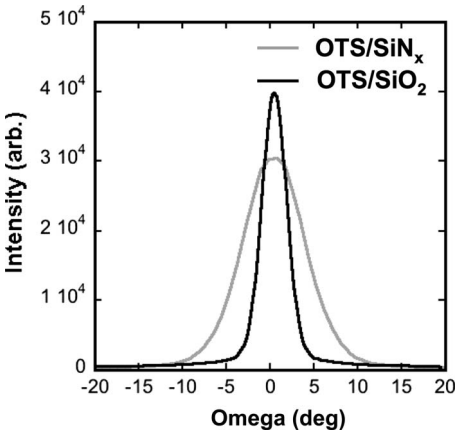

FIG. 17. Wide-angle rocking curve of the (100) Bragg peak of PQT-12 deposited on SiN_x and thermal SiO_2. Both surfaces were treated with OTS prior to the deposition of the semiconductor.

to nucleate crystallites with such tight angular distribution about the surface normal.

Due to its relatively narrow FWHM, we hypothesize that the peak due to well-oriented crystallites measured in the wide-angle rocking curves reflects the angular distribution of crystallites located at the dielectric interface as well. We measured the rocking curve of the (100) peak of PQT-12 spun on SiN_x. The SiN_x was deposited by plasma-enhanced chemical vapor deposition and provides a rougher polymer/dielectric interface (approximate rms roughness of 0.5 nm with a maximum peak to valley roughness of 2.1 nm). Since the polymer film is several tens of nanometers thick, the roughness of the polymer/air interface is not expected to depend on a change in dielectric roughness on the order of a few nanometers. The correlation of the width of the rocking curve with dielectric roughness (Fig. 17) supports our model that this component arises from crystallites at the interface. Similar results have also been observed in films of polythienthiophenes.[38]

The decrease in the FWHM of the wide-angle rocking curve of the (100) peak of PQT-12 on OTS/SiO_2 on annealing, in addition to the suppression of the peak wings and the disappearance of the isotropic crystallite population, shows that the total orientation spread of the crystallites decreases. Moreover, the intensity increase in the resolution-limited peak in the rocking curves of the (200) peaks of both PQT-12 and nPQT-12 on OTS/SiO_2 indicates an increase in the perfectly oriented crystallite population. Overall growth of crystalline fraction can be observed by the comparison of the as-spun and annealed (200) pole figures for PQT-12 (Figs. 14 and 15). On SiO_2/OTS, the increase in intensity of the perfectly oriented and well-oriented domains results in a larger value of integrated intensity and therefore higher crystallinity in PQT-12 after annealing.

Reorientation of the crystalline domains and growth of highly textured crystallites should lead to improvement in charge transport. The large increases in the diffraction signal of perfectly and well-oriented crystallites seen in the (200) pole figure confirm the growth of crystallites with relatively small intergranular tilt through the thickness of the film. As the crystallites rearrange and become better aligned with respect to the common substrate, they also become better aligned with respect to each other. Thus, annealing has a large impact on intergrain transport. It should be noted that the near-normal intensity of the (200) peak increases in PQT-12 by a much larger amount than in nPQT-12 reflecting the relatively larger improvement in transport upon annealing of PQT-12 with respect to nPQT-12. Thus the effect of annealing can be summarized as an increase in the number of both perfectly oriented and highly oriented crystallites accompanied by a decrease in the grain-to-grain out-of-plane misorientation of these crystallites. In addition, the amount of disordered material decreases upon annealing. This is seen by the disappearance of the scattering peak due to disorder in the specular diffraction pattern [Fig. 3(b)] and the smaller integrated intensity of the as-spun pole figures.

The analysis of microstructural changes is in agreement with the electrical characterization of as-spun and annealed PQT-12 films on OTS/SiO_2. Indeed, it was found that annealing did not influence crystalline mobility or the total trap density but tightened the trap energy distribution (Table II). X-ray diffraction indicates that crystallites do not grow in the plane of the substrate upon annealing, therefore the number of traps and the crystalline domain size in the plane of charge transport are roughly unchanged. However, reducing the distribution of crystallite misorientation about the surface normal, as well as reducing the amount of disordered material between the grains, is expected to lead to a reduction in the number of deeper traps, which is equivalent to a tightening of the trap distribution.

The changes in films of nPQT-12 after annealing show some differences from PQT-12. In contrast to PQT-12, the high-resolution GIXS data show an increase in the intensity of the peaks that are in the as-spun films and a slight narrowing of the peak widths. The ratio of the two π-π stacking peaks is not constant and varies slightly depending on the substrate. Interestingly there is a strong reduction in the intensity of the sharp peak at 1.5 $Å^{-1}$ relative to the peaks at 1.65 and 1.7 $Å^{-1}$. As noted previously, there is evidence from the specular scattering that the annealed films comprise two crystalline polymorphs suggesting that the peak at 1.5 $Å^{-1}$ may be associated with the molecular packing in the as-spun films. It is possible that since the crystalline domains have a stronger orientation in the annealed films the changes in intensity of the peaks are due to reorientation of the center of their scattering toward $\mathbf{q}_z=0$. However, the pole figures of nPQT suggest that this is not the case. The rocking curve obtained by imaging the 2D scattering from the (200) peak shows that the as-spun film has some perfectly oriented domains. After annealing the scattering at $\mathbf{q}_{x,y}=0$ from the perfectly oriented crystallites it increases as well as that from the well-oriented crystallites. This increase in intensity suggests that new domains are forming or defects are being removed from partially ordered domains during annealing. We conclude that the mobility increase in nPQT-12 on OTS/SiO_2 upon annealing is probably mostly due to the in-plane growth of crystallite size.[17,25]

B. Effect of the chemistry of the dielectric surface

As mentioned above, the final microstructure in thin films formed via spin coating is kinetically limited. Annealing can

help give polymer chains the mobility needed to rearrange into a more thermodynamically desirable structure. It has been shown that some surface treatments may have the same effect. The low interface energy due to the alkyl chains of the OTS monolayer can provide enhanced mobility of the polymer chains during the deposition process, resulting in a more crystalline film.[43] It is also possible that the interaction between the alkyl chains of the polymer and the methyl terminations of the OTS chains helps the crystallization of the polymer. It should be noted however that our OTS layers did not display any diffraction in GIXS, which suggests strongly that they are amorphous. By comparing the diffraction scans from a PQT-12 film on bare SiO_2 and the corresponding scans from a film on OTS/SiO_2, we investigate the effect that the low surface-energy OTS monolayer has on a PQT-12 thin film.

For the PQT-12 as-spun films, the presence of the OTS monolayer promotes crystallization and reorganization of the polymer. Indeed, both the as-spun and annealed PQT-12 films on SiO_2 show weaker diffraction intensities compared to those spin-coated on OTS/SiO_2. Referring to the high-resolution specular scans, the as-spun film on bare oxide shows very little Bragg diffraction, while the as-spun on the OTS-treated sample exhibits three orders of $(h00)$ peaks. Combining these scans with the corresponding 2D diffraction patterns and complete pole figures, we conclude that both films exhibit the formation of crystallites with appropriate texture, but the OTS monolayer allows for more crystallization to occur regardless of heat treatment (Fig. 18).

The shapes of the specular and 2D patterns after annealing indicate that the crystallites in the films have a similar texture and overall structure (Fig. 2). Both scans show three orders of $(h00)$ peaks and no detectable disorder peak. However, the difference in intensity implies a difference in the crystalline diffracting material present either with regard to crystallite size or the film's percent crystallinity. As mentioned previously, from Fig. 16 the crystallite size can be estimated at approximately 50 nm in the film thickness direction for the annealed film on SiO_2. This is not significantly different from the estimated 70 nm thickness of the crystallites for the OTS-treated annealed film. The intensity difference therefore does not arise from the surface-normal coherence length of the crystallites. Instead, the difference must arise from the relative percent crystallinity. The accurate quantitative assessment of crystallinity in nPQT-12 and PQT-12 as a function of processing conditions is beyond the scope of this paper and will be addressed in a later publication. Nevertheless, our pole figures allow a comparison of the total crystallinity across different films. The PQT-12 films on OTS owe their higher percent crystallinity to the faster surface diffusion of the molecules on the low-energy surface, encouraging self-assembly and crystallization. Additional contributions to increased intensity may arise from the slightly tighter packing in the molecular stacking direction when the film is on OTS, indicated by slightly higher values of q for the $(h00)$ peaks in the specular curves for annealed on OTS when compared to annealed on SiO_2.

The microstructural characterization is in agreement with the electrical characterization and modeling according to the ME model. First, unannealed films of PQT-12 on untreated

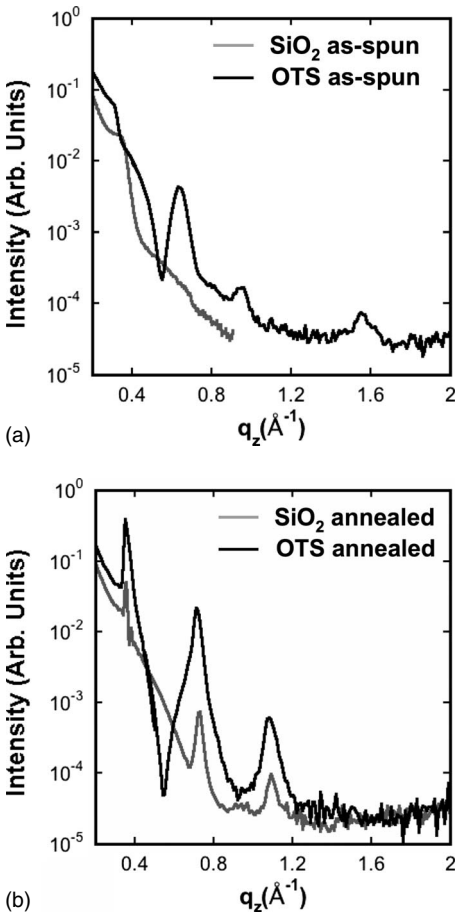

FIG. 18. Comparison of specular diffraction patterns of PQT-12 on OTS/SiO_2 and bare SiO_2 prior to (a) annealing and (b) after annealing.

SiO_2 barely show any field effect, in agreement with the poor crystallinity of these films. The lower percent crystallinity in PQT-12 on bare SiO_2 compared to OTS/SiO_2 implies the presence of a larger fraction of disordered material on the untreated dielectric. In addition to this, rocking curves of as-spun and annealed PQT-12 on SiO_2 illustrate weak crystallite reorganization on annealing, while PQT-12 on OTS showed significant reorganization. These two observations would lead one to expect a broader trap distribution and a larger total trap density for PQT-12 on SiO_2. The decrease in crystalline mobility (μ_0) may be partly explained by the difference in packing density of the lamellar layers, as mentioned above; this difference in d spacing however is small. An additional reason for the decrease in μ_0 may be related to the assumptions of the ME model. The ME model assumes that the DOS is continuous throughout the film, which implies that there are enough crystallites in the film to form continuous paths from source to drain. In PQT-12 on bare SiO_2 the crystallite density is lower than on OTS/SiO_2. We speculate that on the untreated dielectric the crystallite density is below the percolation limit. Thus in order to cross the TFT channel charge must always travel through amorphous regions. As a result the apparent crystalline mobility in the ME model is an average value between the true crystalline mobility and the mobility in the amorphous regions. It

should be pointed out that in such a situation the ME model does not rigorously apply.

In contrast to PQT-12, the nanoparticle dispersion, nPQT-12, comprises organized colloidal aggregates. As-cast films of nPQT-12 show similar x-ray scattering on both SiO_2 and OTS/SiO_2. In particular, on bare SiO_2 nPQT-12 films generally show stronger scattering than those from PQT-12. This feature is expected as the preorganized aggregates likely directly adsorb onto the dielectric surface. The observed field-effect mobility in the as-cast state does not depend on substrate (Table I); this together with the diffraction data suggests that the amount of ordered and disordered materials is independent of the substrate. After annealing the crystallinity of films of nPQT-12 on both SiO_2 and OTS/SiO_2 improves, but the field-effect mobility of films on the former is lower. Since the crystalline domains increase in size on both substrates, this suggests that the difference in mobility is due to intergrain transport. The details of the ordering process are likely to be different on OTS/SiO_2 and SiO_2 interfaces. In the former case, the OTS layer is unlikely to be perfectly ordered itself as it is known that shorter alkane chain length molecules do not form highly ordered SAMs.[44] The conformation of the side chains of the PQT-12 molecules nearest to the dielectric is likely dictated by the defects in the SAM; for instance, if there are missing surface attached alkyl chains, the alkyl side chains of PQT-12 may intercalate into the SAM. In the case of SiO_2, there are no alkyl units with which the side chains of the PQT-12 molecule closest to the dielectric can interact, so the side chains nearest to the surface must have a different conformation than those in the bulk. Minor packing defects such as the tilt of the conjugated backbones can cause states to appear in the electronic gap;[31,45,46] since the side chain ordering promotes the three-dimensional registry, their interactions with the substrate interface may influence the electronic structure of the intergrain material.

These results show that while x-ray scattering can provide information about the characteristics of the molecular ordering in films of semiconducting polymers, it cannot definitively predict the electrical properties. The complexity of the interplay between transport in ordered and disordered domains and between misoriented ordered domains is difficult to capture using most characterization methods. Relatively small changes in molecular conformation can have large effects on the electronic structure. For example, changes in the π-stacking distance and defects due to conformational differences in the thiophene rings in the chain, such as 180° rotations, will both affect the band structure of the crystalline domains. The number of such defects necessary to influence transport is quite small and can be estimated from TFT measurements to be of the order of 10^{19} cm^{-3}. These levels are difficult to characterize using most conventional spectroscopic methods as well as x-ray scattering.

C. Summary of the differences between PQT-12 and nPQT-12

In this work we have examined the changes in the microstructure of films of the same polymer deposited from different starting conditions. The nPQT-12 solution is a dispersion of ~5–10 nm crystalline nanoparticles of PQT-12 and dissolved polymer molecules, while the PQT-12 solution is exclusively made of dissolved polymer molecules. By comparing the changes upon annealing we can deduce some aspects of the film formation process. The main difference between nPQT-12 and PQT-12 in the microstructure evolution upon annealing is observed in the GIXS pattern. The in-plane crystallinity of as-spun PQT-12 films is similar to that of annealed nPQT-12 films and remains virtually unchanged upon annealing. The intensity of the in-plane π-stacking peaks in nPQT-12, on the other hand, increases independent of the interface energy. We conclude that nPQT-12 crystallites grow not only in the film thickness direction—as with PQT-12—but also change in the plane of the film. We attribute this difference to the presence of the nanocrystallites in the nPQT-12 film. These domains may provide partial ordering of the polymer molecules between them in the as-cast film. Annealing at a temperature close to the melting point for several minutes allows the in-plane crystallization process to occur. The increase in crystallite size with annealing time was indeed observed by AFM.[27] It is also likely that the nanoparticles do not all touch the substrate and may trap free polymer molecules underneath them leading to misorientation relative to the surface normal. The breadth of the pole figures is more pronounced in nPQT-12 films than in PQT-12 films in agreement with this hypothesis. Upon annealing, in addition to the perfectly oriented crystallites, the population of well-oriented crystallites ($\pm 15°$ from the normal) grows in nPQT-12 more than in PQT-12, which suggests that these crystallites grow from bulk-located nuclei: the pre-existing nanocrystallites. A very similar arcing is observed on both OTS and bare SiO_2 surfaces further hinting at a bulk effect where the semiconductor/dielectric interface plays little or no role (Figs. 7 and 13). From our x-ray data we thus infer that after annealing the microstructure and the performance of PQT-12 and nPQT-12 films are similar, the path to obtain that microstructure is different in both films, and these differences are summarized schematically in Fig. 19

The impact of the solution used for deposition on charge transport is pronounced. On OTS/SiO_2, the as-cast films of PQT-12 and nPQT-12 have measurable mobilities with the latter being significantly larger. On SiO_2, the as-cast film of PQT-12 does not typically have a measurable mobility whereas that from nPQT-12 is nearly the same as that on OTS/SiO_2. These data show that preorganization of the polymer molecules can reduce the influence of the surface energy of the gate dielectric on the performance of TFTs from as-cast films. After thermal annealing, both PQT-12 and nPQT-12 TFTs on OTS/SiO_2 and SiO_2 have nearly the same field-effect mobility with the former producing the highest values. The annealing process allows the polymer to reorganize under the influence of the interface with the dielectric and produce a high mobility film with the alkylated substrate. Thus, judicious choice of the solution used for deposition and thermal treatment can produce the best mobility possible for a given dielectric.

V. CONCLUSIONS

Charge transport in semicrystalline polymeric semiconductors is governed by different phenomena at different

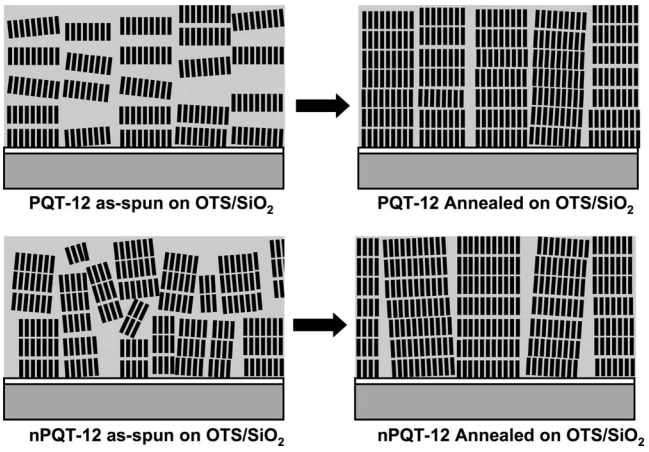

FIG. 19. Evolution of the microstructure of PQT-12 (top panel) and nPQT-12 (bottom panel) upon annealing. The short vertical black lines represent a polymer chain seen end on. Crystallites are formed by stacking the chains vertically (i.e., along the alkyl stacking direction) or horizontally (i.e., along the π-π stacking direction).

length scales. At the mesoscale, charge transport is a property of the microstructure of the polymeric thin film: it is governed by the complex interplay between crystallites and disordered regions in the film. The microstructure of the film and hence the mobility of charge carriers depend strongly on the state of the polymer in the casting solution and on how the semiconducting film is processed. In this work, the microstructure of the crystallites in PQT-12 thin films was thoroughly characterized by synchrotron-based x-ray diffraction.

The as-spun films made from nPQT-12 (a nanocrystallite dispersion) were more crystalline than those made from a polymer solution (PQT-12) independent of the dielectric/semiconductor interfacial energy. As a consequence, carrier mobility in as-spun nPQT-12 films is higher than that in PQT-12. A higher surface-energy dielectric inhibited the crystallization of as-spun PQT-12 during solvent evaporation while it had little effect on the crystallinity of nPQT-12. Consequently, carrier mobility in as-spun films of nPQT-12 on high and low surface-energy dielectrics was identical. Annealing the films always improved crystallite size and for OTS-treated substrates improved intergranular orientation as well. In nPQT-12 films, crystals grew in the plane of the substrate and normal to the substrate direction, while in PQT-12 films crystals only grew in the out-of-plane direction but reoriented themselves and improved their connectivity. With the exception of nPQT-12 films on untreated SiO_2—a high-energy interface—thermal annealing improved the charge transport characteristics of the semiconducting polymer.

X-ray diffraction is a very powerful characterization tool that has proven to be successful in enhancing our understanding of charge transport mechanisms in polymeric semiconductors. In order to successfully correlate carrier mobility with the crystalline microstructure of the film, specular and in-plane diffraction patterns must be collected in addition to rocking curves. It should be however noted that diffraction primarily probes crystalline regions of the film. Therefore, when transport is limited by the disordered regions, other techniques must be employed to gain a complete understanding of the structure-property relationships in this class of materials.

ACKNOWLEDGMENTS

Portions of this research were carried out at the Stanford Synchrotron Radiation Laboratory, a national user facility operated by Stanford University on behalf of the U.S. Department of Energy, Office of Basic Energy Sciences. B. S. Ong and Y. Wu of Xerox Research Centre of Canada are gratefully acknowledged for providing PQT-12 and nPQT-12. The authors acknowledge useful discussion with R. A. Street and J. E. Northrup of PARC and R. J. Kline of NIST. A.S. and L.H.J. gratefully acknowledge financial support from the National Science Foundation.

*Corresponding author; asalleo@stanford.edu

[1] *Organic Light Emitting Devices: Synthesis, Properties, and Applications*, K. Müllen and U. Scherf (Wiley, Weinheim, 2006).
[2] K. M. Coakley and M. D. McGehee, Chem. Mater. **16**, 4533 (2004).
[3] M. L. Chabinyc and A. Salleo, Chem. Mater. **16**, 4509 (2004).
[4] H. Sirringhaus, Adv. Mater. (Weinheim, Ger.) **17**, 2411 (2005).
[5] A. Salleo, Mater. Today **10**, 38 (2007).
[6] H. Sirringhaus, P. J. Brown, R. H. Friend, M. M. Nielsen, K. Bechgaard, B. M. W. Langeveld-Voss, A. J. H. Spiering, R. A. J. Janssen, E. W. Meijer, P. Herwig, and D. M. de Leeuw, Nature (London) **401**, 685 (1999).
[7] H. Sirringhaus, R. J. Wilson, R. H. Friend, M. Inbasekaran, W. Wu, E. P. Woo, M. Grell, and D. D. C. Bradley, Appl. Phys. Lett. **77**, 406 (2000).
[8] Z. Bao, A. Dodabalapour, and A. J. Lovinger, Appl. Phys. Lett. **69**, 4108 (1996).
[9] R. D. McCullough, Adv. Mater. (Weinheim, Ger.) **10**, 93 (1998).
[10] R. J. Kline, M. D. McGehee, and M. F. Toney, Nat. Mater. **5**, 222 (2006).
[11] H. Yang, T. J. Shin, Z. Bao, and C. Y. Ryu, J. Polym. Sci., Part B: Polym. Phys. **45**, 1303 (2007).
[12] H. Yang, T. J. Shin, L. Yang, K. Cho, C. Y. Ryu, and Z. Bao, Adv. Funct. Mater. **15**, 671 (2005).
[13] J. F. Chang, J. Clark, N. Zhao, H. Sirringhaus, D. W. Breiby, J. W. Andreasen, M. M. Nielsen, M. Giles, M. Heeney, and I. McCulloch, Phys. Rev. B **74**, 115318 (2006).
[14] R. J. Kline, M. D. McGehee, E. N. Kadnikova, J. Liu, and J. M. J. Frechet, Adv. Mater. (Weinheim, Ger.) **15**, 1519 (2003).
[15] R. J. Kline, M. D. McGehee, E. N. Kadnikova, J. Liu, J. M. J. Frechet, and M. F. Toney, Macromolecules **38**, 3312 (2005).
[16] A. Zen, J. Pflaum, S. Hirschmann, W. Zhuang, F. Jaiser, U. Asawapiron, J. P. Rabe, U. Scherf, and D. Neher, Adv. Funct. Mater. **14**, 757 (2004).

[17] R. Zhang, B. Li, M. C. Iovu, M. Jeffries-EL, G. Sauvé, J. Cooper, S. Jia, S. Tristram-Nagle, D. M. Smilgies, D. N. Lambeth, R. D. McCullough, and T. Kowalewski, J. Am. Chem. Soc. **128**, 3480 (2006).
[18] M. J. Banach, R. H. Friend, and H. Sirringhaus, Macromolecules **37**, 6079 (2004).
[19] D. M. DeLongchamp, B. M. Vogel, Y. Jung, M. C. Gurau, C. A. Richter, O. A. Kirillov, J. Obrzut, D. A. Fischer, S. Sambasivan, L. J. Richter, and E. K. Lin, Chem. Mater. **17**, 5610 (2005).
[20] A. Salleo, M. L. Chabinyc, M. S. Yang, and R. A. Street, Appl. Phys. Lett. **81**, 4383 (2002).
[21] T. J. Prosa, J. Moulton, A. J. Heeger, and M. J. Winokur, Macromolecules **32**, 4000 (1999).
[22] T. J. Prosa, M. J. Winokur, J. Moulton, P. Smith, and A. J. Heeger, Macromolecules **25**, 4364 (1992).
[23] M. C. Gurau, D. M. Delongchamp, B. M. Vogel, E. K. Lin, D. A. Fischer, S. Sambasivan, and L. J. Richter, Langmuir **23**, 834 (2007).
[24] B. S. Ong, Y. Wu, P. Liu, and S. Gardner, J. Am. Chem. Soc. **126**, 3378 (2004).
[25] B. S. Ong, Y. Wu, P. Liu, and S. Gardner, Adv. Mater. (Weinheim, Ger.) **17**, 1141 (2005).
[26] Y. Wu, P. Liu, B. S. Ong, T. Srikumar, N. Zhao, G. Botton, and S. Zhu, Appl. Phys. Lett. **86**, 142102 (2005).
[27] N. Zhao, G. A. Botton, S. Zhu, A. Duft, B. S. Ong, Y. Wu, and P. Liu, Macromolecules **37**, 8307 (2004).
[28] T. N. Ng, J. A. Marohn, and M. L. Chabinyc, J. Appl. Phys. **100**, 084505 (2006).
[29] A. Salleo, T. W. Chen, A. R. Volkel, Y. Wu, P. Liu, B. S. Ong, and R. A. Street, Phys. Rev. B **70**, 115311 (2004).
[30] R. J. Kline, D. M. DeLongchamp, D. A. Fischer, E. K. Lin, L. J. Richter, M. L. Chabinyc, M. F. Toney, M. Heeney, and I. McCulloch, Macromolecules **40**, 7960 (2007).
[31] J. E. Northrup, Phys. Rev. B **76**, 245202 (2007).
[32] J.-F. Chang, H. Sirringhaus, M. Giles, M. Heeney, and I. McCulloch, Phys. Rev. B **76**, 205204 (2007).
[33] C. Tanase, E. J. Meijer, P. W. M. Blom, and D. M. deLeeuw, Phys. Rev. Lett. **91**, 216601 (2003).
[34] T. J. King, M. G. Hack, and I. W. Wu, J. Appl. Phys. **75**, 908 (1994).
[35] W. B. Jackson, C. C. Tsai, and S. M. Kelso, J. Non-Cryst. Solids **77-78**, 281 (1985).
[36] B. J. Factor, T. P. Russell, and M. F. Toney, Macromolecules **26**, 2847 (1993).
[37] M. F. Toney, T. C. Huang, S. Brennan, and Z. Rek, J. Mater. Res. **3**, 351 (1988).
[38] M. L. Chabinyc, M. F. Toney, R. J. Kline, I. McCulloch, and M. Heeney, J. Am. Chem. Soc. **129**, 3226 (2007).
[39] M. Ballauff, Angew. Chem., Int. Ed. Engl. **28**, 253 (1989).
[40] B. E. Warren, *X-Ray Diffraction* (Addison-Wesley, Reading, MA, 1969).
[41] C. Tanase, E. J. Meijer, P. W. M. Blom, and D. M. deLeeuw, Org. Electron. **4**, 33 (2003).
[42] R. E. Geer, R. Shashidhar, A. F. Thibodeaux, and R. S. Duran, Phys. Rev. Lett. **71**, 1391 (1993).
[43] M. M. Despotopoulou, C. W. Frank, R. D. Miller, and J. F. Rabolt, Macromolecules **29**, 5797 (1996).
[44] S. R. Wasserman, Y.-T. Tao, and G. M. Whitesides, Langmuir **5**, 1074 (1989).
[45] D. M. DeLongchamp, R. J. Kline, E. K. Lin, D. A. Fischer, L. J. Richter, L. A. Lucas, M. Heeney, I. McCulloch, and J. E. Northrup, Adv. Mater. (Weinheim, Ger.) **19**, 833 (2007).
[46] R. A. Street, J. E. Northrup, and A. Salleo, Phys. Rev. B **71**, 165202 (2005).